



ELSEVIER

Contents lists available at [ScienceDirect](#)

International Journal of Marine Energy

journal homepage: www.elsevier.com/locate/ijome



Energy efficiency of pneumatic power take-off for wave energy converter



Matthias Liermann*, Omar Samhoury, Samer Atshan

American University of Beirut, Department of Mechanical Engineering, Fluid Mechatronics Lab, P.O. Box 11-0236, Riad El Solh, Beirut 1107-2020, Lebanon

ARTICLE INFO

Article history:

Received 9 January 2015

Revised 1 October 2015

Accepted 15 October 2015

Available online 26 October 2015

Keywords:

Wave energy converter

Air power

Small scale

Power transmission

Fluid power

Energy efficiency

ABSTRACT

This paper investigates the energy efficiency of a pneumatic power transmission which serves as power take-off for a small-scale, low cost, portable wave energy converter. The wave energy converter was implemented and tested as a prototype in the Eastern Mediterranean. The power transmission uses a standard cylinder as a pump with check valves for flow rectification. Air is stored in an accumulator and discharged through a vane motor coupled to a brushed DC generator which is connected to an electrical load. Numerical models are given for each component of the system which allow to calculate the component and system losses for a range of operating conditions.

Experimental results are presented from laboratory tests with the power take-off system. Measurements are conducted at steady state, transient, as well as simulated wave conditions using a hydraulic wave simulator. The measurements validate the predicted losses of the numerical models. The losses in each part of the power transmission are graphically illustrated with a Sankey diagram. We conclude that even though the overall efficiency is low, the setup serves well as a low cost instructional tool to teach principles of wave energy harvesting and to demonstrate typical challenges faced in the design of wave energy converters and pneumatic power transmission.

© 2015 Elsevier Ltd. All rights reserved.

* Corresponding author. Tel.: +961 1 350000x3497.

E-mail address: matthias.liermann@aub.edu.lb (M. Liermann).

1. Introduction

The power take-off of a wave energy converter (WEC) is an integral part of its design. Its damping characteristic determines the motion of the WEC and therefore, not only does it have an effect on the downstream energy transmission but also on the primary power transfer from the wave into the oscillating body. There exist a variety of power take-off mechanisms based on hydraulics, linear electrical generators, and turbines [1,2]. Most power take-off mechanisms which were developed for WECs are based on hydraulics, where the oscillating primary motion is transferred into hydrostatic pressure and transformed through fluid power drives into useful shaft motion for electricity generation [3,4]. The purpose of our study was to assess the efficiency of a pneumatic power transmission consisting of a pneumatic piston, accumulator and a pneumatic motor. The concept was developed as a prototype for teaching fluid power systems and the control of wave energy converters. Following this introduction we present the wave energy converter prototype and its pneumatic power-train. In Section 3 we develop the loss models for each part of the drive train and estimate the overall efficiency. Section 4 gives an overview of the laboratory system setup and presents measurement results which support the theoretical model.

2. WEC prototype and pneumatic power-take-off

The wave energy converter prototype was designed at the American University of Beirut (AUB) with the objective to harvest 20 W of electrical power from average wave conditions at the beach of AUB. No specific data existed about the wave resource of this location. The Wind and Wave Atlas of the Mediterranean Sea [5] provides an estimate of the wave resource at a distance of 233 km. Measured wave buoy data is given for the airport of Beirut in [6]. The mean spectral significant wave height for the measurement period between 2000 and 2003 was $H_{m0} = 0.7$ m and the mean period was $T_{m02} = 4.21$ s. For comparison, the wave energy flux per unit crest of a regular deep water wave with such a significant wave height and period is $P \approx 0.49H_s^2T_e = 1.28$ kW/m. From visual observation of the waves at the intended deployment site the significant wave height and period was determined as $H_s = 0.6$ m and $T_s = 7$ s, which corresponds to approximately the same energy flux.

The setup was designed to be portable and easily deployable for testing. The intended site of deployment at the beach of Beirut is rocky and has reefs whose tops are almost flat and level with the mean water line. The electrical components were planned to be placed apart from the primary power take-off, outside the water, easily accessible from the beach. A pneumatic transmission was chosen for the primary power take-off to resemble the structure of a hydraulic power take-off. Off-the-shelf industrial components were used for the pneumatic system. The choice was mainly made because hydraulic motors do not commercially exist for such a low-power application. Pneumatic drives generally have a lower stiffness and efficiency compared to hydraulic drives due to the compressibility of the medium air and associated thermal losses. Pneumatic power transmission for WECs are also found in Oscillating Water Column (OWC) type devices, though at lower pressures and higher flow rates [7]. OWC WECs use bi-directional Well's turbines to generate electricity. One might assume that the compressibility of air is a disadvantage to the primary power capture. However, as studies for OWC type devices show, the compressibility or the air column in an OWC WEC does not have a large effect on annual yield, given that the power take-off system can provide an optimal damping for each considered configuration [8].

The WEC design presented in this study consists of a square fibre-glass coated styro-foam 208 L float attached to a beam which is hinged on the lower part of the power take-off steel frame as shown in Fig. 1. The other end of the beam is connected to the piston rod of a pneumatic cylinder with 0.92 L maximum displacement and 0.125 m stroke length. The cylinder operates with two check valves as a single-stage air pump. Air is stored in a 5 L accumulator. The accumulator size is chosen in relation to the cylinder size. The aim is to be able to store the energy of two wave periods at a reasonable low increase of pressure. Assuming isothermal compression at $T_0 = 20$ °C, the increase in pressure in the accumulator is only 3.7 kPa. The accumulator is connected via a 12 mm diameter hose to the

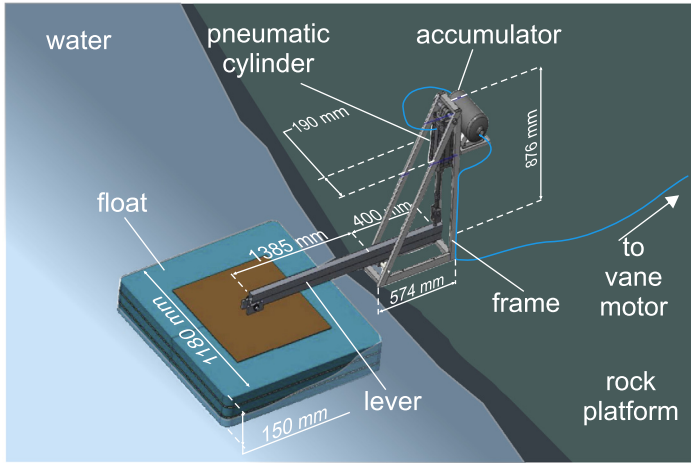


Fig. 1. WEC prototype mounted of rock platform.

motor-generator unit. The motor-generator unit is situated in a protected and dry area on the beach, where easy monitoring of the device is possible. The light design of the float results in easy handling of the portable setup. However, as a consequence, only the heave upward motion energy can realistically be harvested by this device. Because the float was designed purely as a wave follower with very high hydraulic stiffness compared to its weight, it can further be predicted that mainly the potential energy contained by the wave is being captured by the float. This reduces the theoretically available energy flux by a factor four to $P_m = 320 \text{ W/m}$. The dimensions of the float were chosen based on the assumption that the total energy efficiency of the power take-off system would be around 5% so as to yield 20 W of electrical output power.

Fig. 2 shows a schematic of the whole system, including power take-off, transmission and electric circuit. The pneumatic system is an open loop system. Air is drawn into the pumping cylinder (c) from the environment through a filter unit (a) and a check valve (b). The filter consists of a particle pre-filter

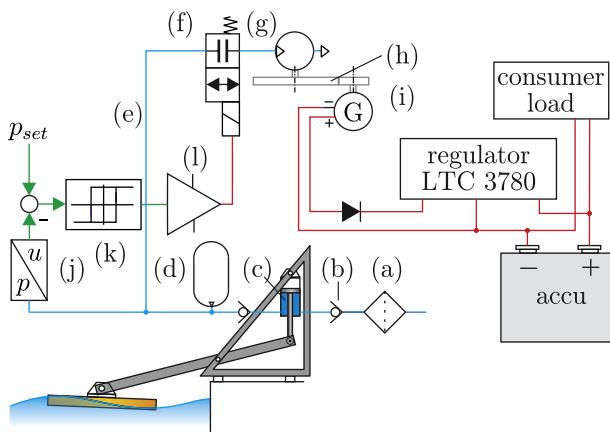


Fig. 2. Complete power transmission of WEC. Details: (a) coalescent and particle filter. (b) check valve. (c) pumping cylinder. (d) accumulator. (e) accumulator line. (f) switch valve. (g) vane motor. (h) belt transmission. (i) DC motor/generator. (j) pressure transducer. (k) hysteresis function to set pressure range at which valve opens. (l) power amplifier.

and a coalescing filter which removes salt-water mist from the intake air which could harm the pneumatic components. Another way to avoid salt water contamination would be to recirculate the air in a closed loop. Air is pumped during upward heave motion of the float and fed through the outlet check-valve into the accumulator line (e). A switch valve (f) controls the flow into a small vane motor (g) with nominal output power of 30 W. The switch valve allows discharge only when the pressure is high enough to allow efficient power transmission. The pressure range in which the valve is opened is determined from the hysteresis function (k) that takes the difference of pressure set-value minus measured pressure from the transducer (j). The motor is connected through a belt transmission (h) to a 24 V brushed DC motor (i), which functions as a generator in this setup. The motor cables are connected to a step-up/down regulator module which produces appropriate voltage to charge a battery. An electrical load is attached in parallel.

3. Mathematical model of losses

In this section we explain the various losses occurring in the power-train from production of pressurized air in the piston pump to consumption of useful electrical energy in the consumer load. The primary energy conversion from wave power to mechanical power at the piston rod has been explained previously [9–12]. The total energy loss in the transmission is the sum of the following major losses:

- Losses in pneumatic motor L_{PM} .
- Losses in generator L_{Gen} .
- Throttling losses of air preparation unit, pipes and switch valve L_{Thr} .
- Thermal and friction losses of pumping cylinder L_{Cyl} .
- Thermal losses of accumulator L_{Acc} .

All losses together sum up to the total loss.

$$L_{tot} = L_{PM} + L_{Gen} + L_{Thr} + L_{Cyl} + L_{Acc} \quad (1)$$

The following subsections explain these losses which occur in all components of the WEC. The thermal losses of the accumulator can be treated in combination with the thermal losses of the cylinder.

3.1. Losses in pneumatic motor

The pneumatic motor in our setup is a small unidirectional 30 W vane motor manufactured by the company Deprag with nominal torque of 0.57 N at nominal speed of 52 rad/s. The nominal pressure is 0.7 MPa. All pressures mentioned in this paper are absolute pressures. At no-load and nominal pressure it spins with 105 rad/s and consumes 100 L/minANR (standard liter). Fig. 3 shows the motor torque, air consumption and efficiency as a function of speed for different supply pressures between 0.4–0.8 MPa extracted from catalog data [13]. The efficiency of the motor is very low. To calculate and plot the efficiency of the motor, the definition for air power by Cai et al. [14] is used:

$$P_{air} = \dot{m}RT_{atm} \left[\ln \frac{p}{p_{atm}} + \frac{n}{n-1} \left(\frac{T}{T_{atm}} - 1 - \ln \frac{T}{T_{atm}} \right) \right] \quad (2)$$

It is assumed that the air at the intake has ambient temperature. The low efficiency of the vane motor matches well with results given in literature [15]. The maximum efficiency is found to be 13.6% for a supply pressure of 0.8 MPa at around 41 rad/s. Although it is unusual to use a vane motor for power transmission, vane motors have some unique advantages which justify their use despite their low efficiency. They have a high power-to-weight ratio, operate at cool temperatures and do not overheat, even in stall condition. Furthermore they are indifferent to dirt and can be used in explosive atmospheres. It is possible to design vane motors with higher efficiency by increasing the expansion ratio and making more use of the expansion energy of the air. However, air expansion causes the outlet air

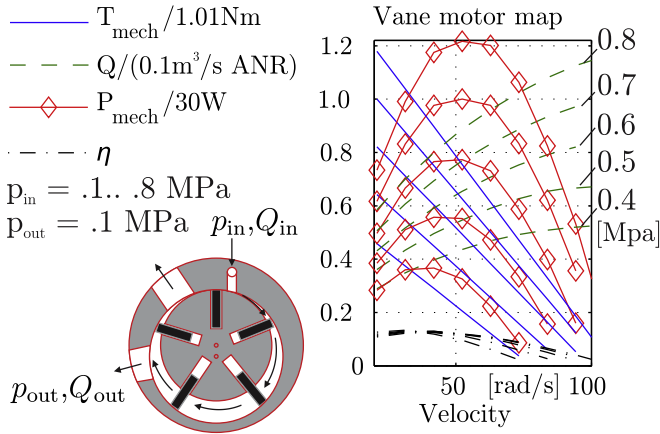


Fig. 3. Torque T_{mech} , air consumption Q , power P_{mech} and efficiency η of pneumatic motor as a function of speed with data derived from [13].

temperature to drop. Considering that, in general, air is supplied at ambient temperature, an expansion ratio of 1.25 is enough to cool down from 25 °C to freezing point (assuming adiabatic expansion). At freezing temperature the air moisture deposits in pipelines and nozzles and leads to clogging. Therefore, the expansion ratio of vane motors is usually designed to be lower than 1.25 and the expansion energy is largely lost. To make the motor more efficient, one could use the seawater to provide heat for the motor. This would allow the design of a larger expansion ratio and prevent the loss of the expansion energy.

3.2. Losses in DC generator

The generator is a 24 V brushed DC permanent magnet motor rated at 40 W electrical power at 188 rad/s. It is connected to the vane motor via belt drive with a transmission ratio of $i = 2.15$. In this paper the DC generator is regarded as a unit with the belt drive. Whenever we refer to the speed of the generator, it is the same shaft speed ω as that of the pneumatic motor. Regarding steady state

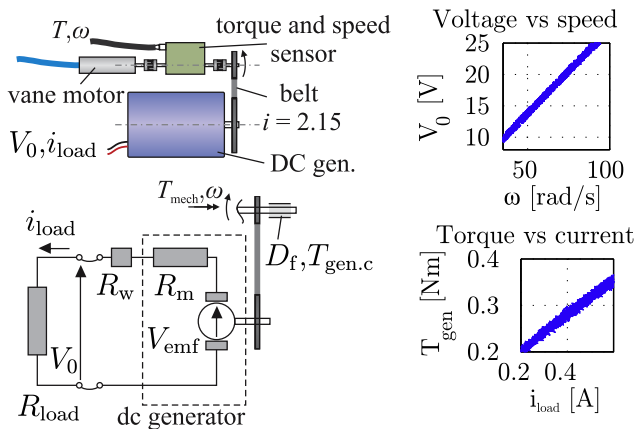


Fig. 4. Motor-generator setup and DC generator steady state performance.

operation we can view the generator as a variable electro-motive force connected to an armature-circuit resistance [16], see Fig. 4.

We can characterize the generator by its electro-motive force constant K_{emf} , which describes the proportionality between its speed ω and armature voltage V_{emf} as well as by its armature resistance R_m . If needed, a separate resistance can be specified for slip-ring connectors and wiring R_w .

$$V_{emf} = K_{emf}\omega \tag{3}$$

$$i_{load} = \frac{V_{emf}}{R_m + R_{load} + R_w} \tag{4}$$

The pneumatic motor is connected to the generator through a synchronizing belt transmission. This transmission adds significantly to the friction of the generator. The generator and transmission friction can be modeled as a static coulomb friction $T_{gen.c}$ with a velocity-proportional rotational damping with damping constant D_f . The static friction component is mainly caused by the meshing of the belt with the gears.

$$T_{gen.fric} = T_{gen.c} + D_f\omega \tag{5}$$

The relationship between the mechanical torque T_{mech} and the generator speed can be expressed using the motor constant K_m as:

$$T_{gen} = T_{gen.fric} + K_m i_{load} \tag{6}$$

Assuming no magnetic losses, electrical and mechanical power can be considered equal, and then $K_m = K_{emf}$. This assumption is often made because the magnetic losses are a function of speed. All losses that are proportional to the speed can be treated in a single damping coefficient D_f , which is dominated by the mechanical friction. Combining Eq. (5) with Eqs. (3)–(5), we can express the overall damping coefficient D_f as:

$$D_f = \frac{T_{gen} - T_{gen.c}}{\omega} - \frac{K_{emf}^2}{R_m + R_{load} + R_w} \tag{7}$$

Using measured data given in Fig. 4, we can calculate the damping constant with values given in Appendix A. Fig. 5 shows on the left side the generator torque versus speed curve of the dc-generator for an exemplary load resistance of $R_{load} = 3 \Omega$. The maximum efficiency is reached for the highest speed and torque. Around the nominal speed of the vane motor (52 rad/s) it reaches

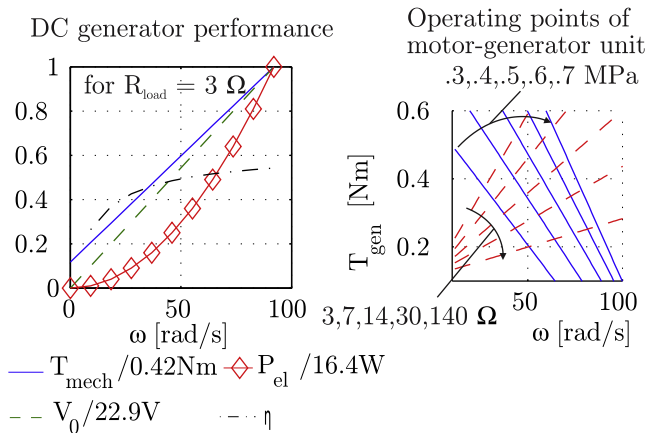


Fig. 5. Left: Performance and efficiency of electric DC generator for exemplary load as a function of speed. Right: operating points are found as the intersection of torque-speed curves of motor and generator. Plot shows these curves for a variety of load resistances and pressures.

around 50%. The operating point of the pneumatic motor coupled to the DC generator is given through the condition that the shaft torque and speed are equal. On the right side of Fig. 5 the torque-speed curves of the motor (solid lines) and the generator (dotted lines) are plotted for a variety of load resistances and supply pressures. An operating point for a certain load and pressure can easily be found from this graph by interpolation.

3.3. Combined losses of fluid-electrical power transmission

By solving for the intersection of motor and generator torque-speed curves, the operating points may be found for the motor and generator. The motor is controlled by applying an inlet pressure p_{in} while the consumed flow is a result of the motor speed. The generator speed is equal to the motor speed. The generator brakes the motor with a torque that is a function of the generator current Eq. (6), while the generator voltage is a function of its speed, Eq. (3). Voltage and current of the generator have a ratio which is fixed by the load resistance connected to the generator. Therefore the power transmitted through the motor/generator unit is governed by the motor pressure and the load resistance. Fig. 6 shows the transmitted power and the overall efficiency of the coupled motor/generator unit as a function of the pressure at the motor and the load resistance applied at the generator. The point of highest efficiency $\eta_{max} = 6.1\%$ is found for a supply pressure of 0.6 MPa and an electrical resistance of 3 Ω . At this combination the speed of the motor is 44 rad/s, with an efficiency of the motor of 12.7% while the generator and belt transmission operates at efficiency of 48.1%. The product of motor and generator efficiencies is the total efficiency.

3.4. Losses in transmission line and valve

The losses in the transmission line, check and switch valve, as well as the air preparation unit are friction losses with turbulent character. While the fluid expands along the negative pressure gradient, the friction and expansion power are of similar magnitude. It can be observed from measurements that the temperature of air stays almost constant while air flows through the tubes. Falkman [17] derived an equation for the pressure drop of air flowing through smooth pipes on the basis of the Bernoulli equation and using Blasius’s pipe friction model. This equation fits very well with empirical models in [18,19].

$$\frac{p_2^2 - p_1^2}{2p_1} + \frac{\lambda L \rho_1 w_1^2}{2D} = 0 \tag{8}$$

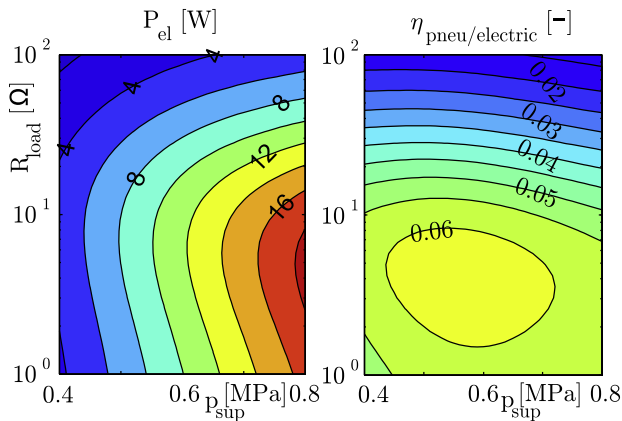


Fig. 6. Left: Transmitted power as a function of load resistance and pressure. Right: total efficiency of fluid-electrical power transmission as a function of load resistance and pressure.

With $p_{1,2}$ inlet and outlet pressure, w_1 and ρ_1 the inlet average speed and density, L and D the length and diameter of the tube, and λ the friction coefficient according to Blasius’s model using the Reynolds number.

$$\lambda = \frac{0.3164}{\text{Re}^{0.25}} \tag{9}$$

$$\text{Re} = \frac{wD\rho}{\mu} \tag{10}$$

Typical dynamic viscosity of air is $\mu = 1.83 \cdot 10^{-5}$ Pa s. It can easily be verified that flow in tubes and other pneumatic components is usually turbulent $\text{Re} > 2300$. The pressure drop in components other than tubes can be modeled as additional sections of tubes of the same diameter as the tubes they are connected to. The length of the tube is calculated using a correction factor K that is listed in literature for different component classes.

$$L_{\text{equiv}} = KD_{\text{tube}} \tag{11}$$

Fig. 7 shows the line sections and components between the piston pump and the vane motor. There are several T-connectors for pressure sensors and thermocouples, a diaphragm switch valve, reducers, a flow sensor, and a filter unit. The tube sizes range between 12 mm at the accumulator and 4 mm at the vane motor inlet. Barber [20, p. 141] gives the values for the correction factors listed in Table 1.

The motor speed and therefore the air flow is determined by the motor inlet pressure and the electrical load, as explained in the previous section. Fig. 7 shows in the left diagram the flow in [L/min ANR] as a function of electrical load and supply pressure. The right diagram shows the power loss L_{Thr} in the line as a result of those flow and pressure conditions. The highest losses occur at the highest flow which corresponds to high pressure and high electrical resistance. Compared to the losses in the motor/generator unit, the losses in the tubes and connectors are very small. For example, at the point of highest efficiency of the motor/generator unit (3Ω and 0.6 MPa) the losses in the motor/generator unit are $L_{\text{Gen}} + L_{\text{PM}} = 169 \text{ W}$ compared to 0.36 W losses in the air transmission.

3.5. Losses in pumping cylinder

The pumping cylinder converts the mechanical force and motion of the oscillating body into pressurized air. The pressurized air is delivered through the outlet check valve only if the cylinder pressure exceeds the accumulator pressure. If the cylinder pressure does not reach and exceed the accumulator pressure, the check valve remains closed and the pressurized air expands in the return motion of the

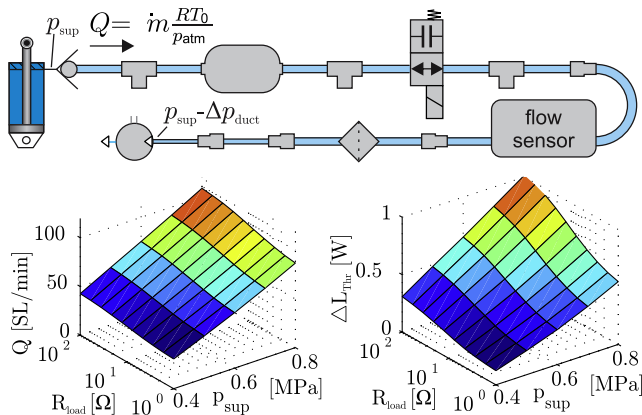


Fig. 7. Losses in transmission line as a function of supply pressure and electrical load.

Table 1

Correction factors to calculate equivalent pipe length for pneumatic components.

Component	K
Run of tee	20
Diaphragm valve fully open	60
Reducer	25
Swing check valve fully open	80
Bend radius = diameter of pipe	16

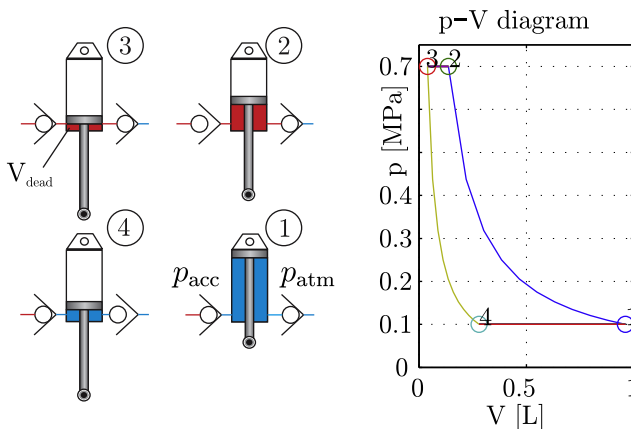
oscillating body. In that case the pneumatic piston temporarily stores the energy supplied by the wave like a spring and returns it to the environment with some thermal and friction losses. The cylinder used in the setup has a displacement volume of 0.92 L and a maximum stroke of 0.125 m.

Two kinds of losses have to be considered for the cylinder: thermal losses and friction losses. The cylinder heats up due to the large compression ratio of the gas inside. Heat transfer through the cylinder body takes place, which represents a loss of energy. Also, friction occurs at guide rings and seals of the cylinder. Losses due to friction can be modeled in a variety of ways. For a detailed overview see [19]. We use an empirical coulomb friction model with dynamic friction according to [21, p. 72].

$$F_{\text{cyl.c}} = 0.4 \frac{\text{N}}{\text{mm}} \cdot D_{\text{piston}} \quad (12)$$

Losses through heat transfer are more complex to describe. The rate of heat transfer not only depends on geometry and material but also on the mixing of the fluid [22]. Sometimes the ideal gas equation for polytropic compression and expansion is used to model the compression in the presence of heat transfer. It has to be noticed, however, that the assumption of a constant polytropic index is not true for a system with varying volume. Another way to take the heat transfer into account is to use a time-domain simulation model with implementation of heat transfer assuming a specific heat transfer coefficient. Whichever way the thermal losses are considered, it is clear that in the setup of the study, the air cools down to ambient temperature before it reaches the motor. Indeed, measurements indicate that the cooling inside the cylinder is very efficient. The air temperature at the outlet of the cylinder only increases by a few degrees C. Therefore, for the sake of simplicity, isothermal compression is considered in the cylinder.

Fig. 8 illustrates the isothermal compression of air in the cylinder chamber. In state 1 the cylinder is fully retracted and filled with air at atmospheric pressure p_{atm} . The compression begins until the

**Fig. 8.** Isothermal compression of cylinder.

cylinder pressure reaches accumulator pressure p_{acc} . Then the outlet check valve opens and air is displaced at accumulator pressure until the cylinder reaches its end of stroke and only the dead volume V_{dead} in the cylinder cushioning and attached tubing is left. The dead volume is then expanded to atmospheric pressure in the back stroke (3–4). In the last stage, the cylinder draws air through the inlet check valve until it is fully retracted. The total consumed mechanical work is the integral $\int p \, dV$. However, technically, the expansion energy (3–4) is not received back as useful form of energy. It only helps to overcome cylinder friction but is not reused for the next compression cycle. Therefore, for the account of energy consumption the expansion (3–4) is replaced by a vertical line from the accumulator pressure down to atmospheric pressure at constant volume as if no expansion would take place. The friction losses are only accounted for the portion of the stroke length when the actuator is providing positive work.

The consumed mechanical work is the sum of compression work plus displacement and friction work. The displacement work is positive when air is displaced against accumulator pressure and negative in the back stroke, where atmospheric pressure is helping.

$$W_{cyl.mech} = W_{compr} + W_{displ} + W_{friction} \tag{13}$$

$$\begin{aligned} &= p_{atm} V_1 \ln \frac{p_1}{p_2} + p_{acc} (V_2 - V_{dead}) \dots \\ &\quad - p_{atm} (V_1 - V_{dead}) + F_{cyl.c} s_{p.max} (2 - s_{exp}) \end{aligned} \tag{14}$$

The friction work is the product of coulomb friction force $F_{cyl.c}$ and the piston travel distance, which is twice the maximum stroke $s_{p.max}$. The portion of travel that is driven by the expansion work is s_{exp} . The consumed power is a function of the wave period T_p :

$$P_{cyl.mech} = \frac{W_{cyl.mech}}{T_p} \tag{15}$$

The cylinder converts mechanical power into pneumatic power. The efficiency of this conversion is the ratio between power output to power input. The output power is air power, calculated according to Eq. (2) assuming ambient temperature. As Fig. 9 shows, the efficiency of compression is between 60 and 95 percent depending on the amount of dead volume left when the piston reaches its end stroke position and depending on the accumulator pressure. With the assumption of isothermal compression, the air that reaches the accumulator is at room temperature and no further losses occur in the accumulator. It can be seen that at a pumping period of $T_p = 5 \text{ s}$ and a dead volume of

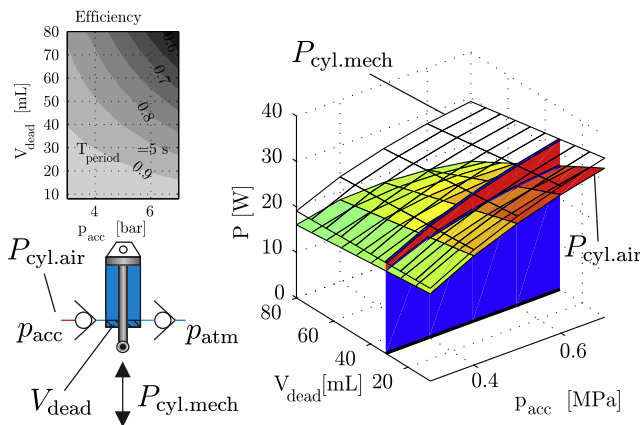


Fig. 9. Power consumed and delivered by cylinder as a function of accumulator pressure and dead volume, assuming an oscillation period of 5 s and full stroke of piston.

$V_{\text{dead}} = 80 \text{ mL}$, only 15 to 17 Watts of pneumatic power are delivered to the accumulator. Clearly, to reach the aim of delivering 20 W of electric output power, the number of working cylinders needs to be increased.

4. Efficiency measurement

In this section we present measurement results to validate the models of the losses given in the previous section. The laboratory setup is depicted in Fig. 10. It consists of a wave simulator in the form of a servo-hydraulic axis connected to the pneumatic piston in the left of the picture. The cylinder pumps air into an accumulator which serves as an intermediary energy storage. The outlet of the accumulator can be closed by a solenoid diaphragm valve. It opens when a sufficient pressure is reached in the accumulator that allows efficient operation of the motor generator unit. Two pressure sensors and thermocouples are employed before and after the switch valve to determine its resistance. A thermal flow sensor and a filter/lubrication unit are connected between the switch valve and the pneumatic vane motor. The vane motor shaft is connected to a synchronizing belt transmission via a torque sensor and an encoder. The brushed DC generator electrical outlet is connected to an adjustable load resistance to simulate different electrical loads.

The measurements are performed in three stages. First, steady state measurements are performed at different constant pressure and load levels. Then transient operation is performed where the accumulator is discharged from its highest pressure 0.7 MPa until stop of the motor. Finally, continuous operation is tested with the servo-hydraulic wave simulator as power source. The first set of experiments verify the theoretical results, at which combination of pressure and electrical load we can expect best efficiency. The second set of experiments provides the “composite” efficiency when the accumulator is discharging and continuously changing its pressure. Because it is not obvious how much air leaves the accumulator at which pressure level, the second set of experiments allows the study of the optimum pressure limits at which operation of the motor should start and stop. In the third type of experiment, the whole power take-off system is operated at simulated constant wave conditions for a longer period. The wave input is a sinusoidal motion with 121 mm stroke and a period of 5 s. In that test, the accumulator is intermittently charged and discharged.

4.1. Steady state operation

In steady state operation the accumulator is connected to the air supply via a pressure reducer valve. The pressure can be adjusted to set levels and for each pressure we connect a series of different

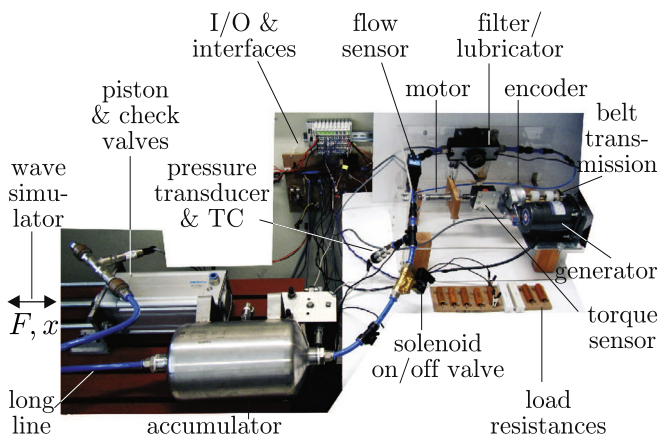


Fig. 10. Laboratory setup to measure energy efficiency of power take-off.

resistances to the generator. The pressure levels are: $p_{\text{sup}} = \{0.3, 0.4, 0.5, 0.6\}$ MPa and the resistance levels are: $R_{\text{load}} = \{147, 47, 28.8, 18.3, 15, 11.1, 9.0, 7.8, 6.8, 6.5, 5.6, 5.4, 4.4\}$ Ω . We measure the power in and out of the major components of the setup, the air transmission, the motor and the generator. The losses can be depicted in a Sankey diagram exemplarily for a certain combination of pressure and electrical load, see Fig. 11. From the theoretical model we would expect an overall efficiency of slightly more than 6% for that operating point, see Fig. 6. Experimentally we get an efficiency of 6.6%. Fig. 12 shows the electrical power output and efficiency for all combinations of supply pressures and loads. The results can be directly compared to Fig. 6. In comparison, the measured efficiency is generally slightly higher than the theoretically predicted one.

4.2. Accumulator discharge operation

The pumping cylinder cannot provide enough air power to allow continuous discharge of the motor. For continuous operation at for example 0.6 MPa and load resistance $R_{\text{load}} = 7.8 \Omega$, the amount of required air power for continuous operation is 208 W, as Fig. 11 demonstrates. A single pumping cylinder may in some cases only provide less than 20 W depending on the wave period and the dead volume of the cylinder, as can be seen from Fig. 9. Therefore, as the wave energy converter prototype is used with only one cylinder, the accumulator will intermittently be charged to a certain pressure level and then discharged. Experiments have been conducted with all applicable electrical loads while discharging from 0.6 MPa until stop of the motor. Fig. 13 shows such a measurement for a load resistance of 4.4 Ω . Each colored surface illustrates the power difference between input and output of a certain section of the system. The losses in check valve, switch valve and ducts are so small that they are illustrated in a magnified section of the plot. The efficiency deteriorates significantly for pressure levels below 0.3 MPa because of the low speed of the generator. The generator comes to a halt for a pressure of 0.2 MPa at this electrical load.

4.3. Complete WEC simulation with sinusoidal excitation

Finally, the charging and discharging of the accumulator is tested with a simulated sinusoidal excitation of the pumping cylinder. A hydraulic servo-axis is used to drive the power take-off cylinder with a stroke of 121 mm and period of 5 s. Fig. 14 shows a section of the charging process for three periods starting from 0.4 MPa. The upper diagram shows the pressure in the pumping cylinder and in the

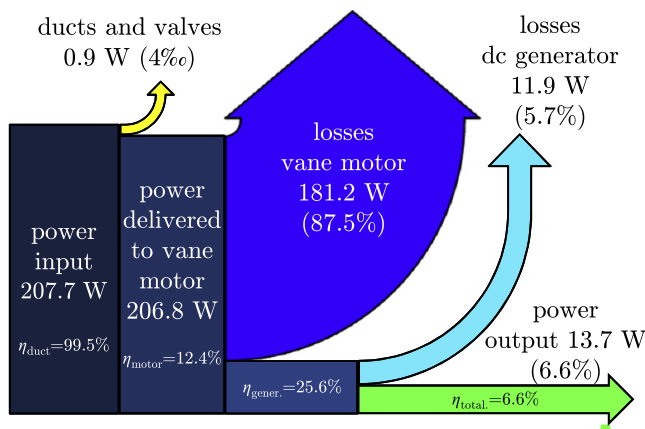


Fig. 11. Exemplary Sankey diagram for steady state operation of power take-off at $p_{\text{sup}} = 0.6$ MPa and $R_{\text{load}} = 7.8 \Omega$.

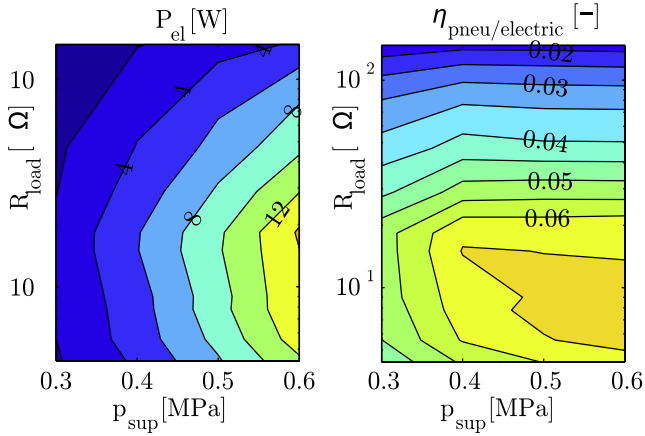


Fig. 12. Measured electrical power output and total efficiency at various input pressures and loads.

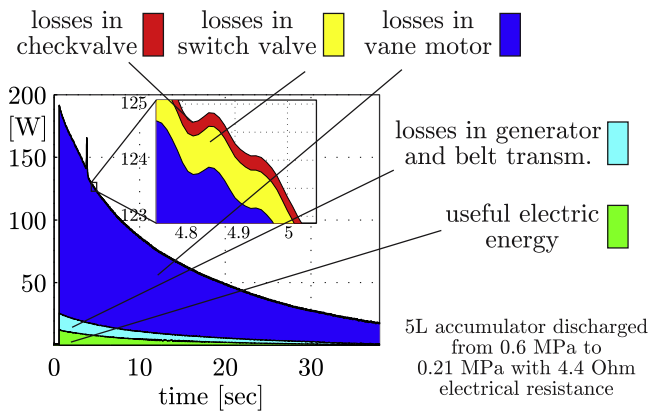


Fig. 13. Power input and losses as a function of time while accumulator discharges.

accumulator. The middle diagram shows the cylinder position and velocity. The bottom diagram shows the air temperature at the outlet of the check valve. The compression occurs nearly, but not quite, isothermal, as the temperature plot indicates. The inner surface of the cylinder is huge compared to the relatively low amount of mechanical power exerted on the cylinder. Expressed quantitatively, while the power peaks are around 110 W for compression at 0.3 MPa, the average power exerted on the air is only 21.8 W. The slow oscillating motion gives plenty of time for cooling. It can be seen from the upper diagram that at 0.4 MPa each period increases the pressure in the accumulator by 8 kPa. Only 121 mm of the theoretical full stroke of 125 mm could be used in the experiment. The remaining 4 mm are probably used up by the elastomeric end stop damper elements. Not being able to use the full stroke resulted in increased dead volume. The comparison with simulation results indicates, that the sum of cylinder dead volume, the volume of the tee connector, fittings and the check valves is nearly 80 mL.

Fig. 15 shows pressure, motion and temperature plots for the discharging process. It is seen that the pumping process continues during discharge. The temperature is plotted in the bottom diagram for

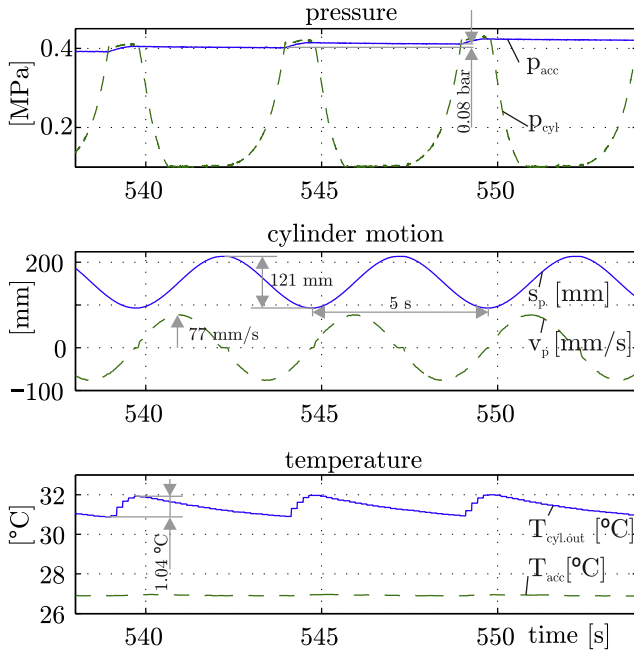


Fig. 14. Charging of accumulator with wave simulation.

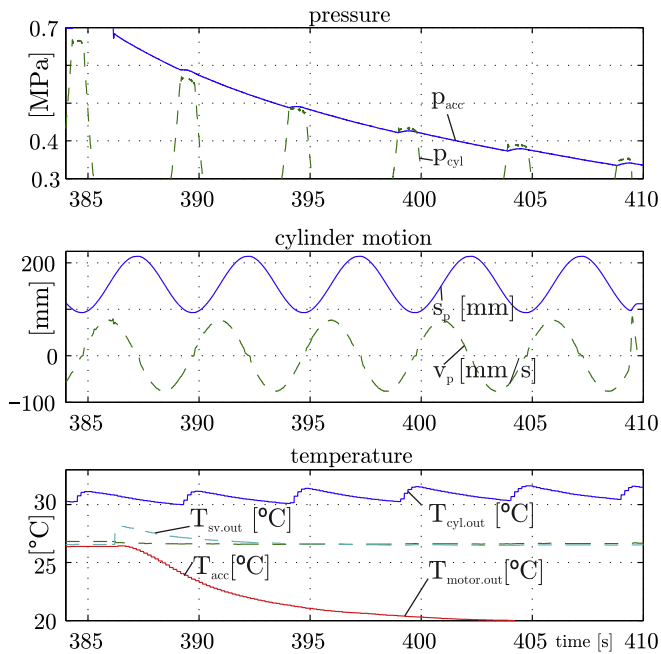


Fig. 15. Discharging of accumulator with wave simulation.

Table 2
Budget of WEC.

Item	Cost US \$
Float	157
Steel frame and lever	122
Cylinder	236
SS accumulator	204
Check valves	18
Air filter	17
Rod eye, bearings, flanges, tubing, fittings etc.	242
Vane motor	998
Generator and electrical components	100
Total	2094

different points in the system. The temperature just behind the switch valve $T_{sv,out}$ increases for a short time after the switching valve opens. This is caused by the compression of air in the line between valve and motor. The incoming compressed air has ambient temperature and soon the temperature at the thermocouple is back to normal. The motor outlet temperature drops only to 20 °C during the short operation period of around 25 s. This demonstrates that only a small fraction of the expansion energy of the compresses air is used to avoid freezing of the motor outlet.

The overall efficiency of the power take-off is the ratio of electrical energy obtained from discharge of a certain pressure difference over the energy used for charging the accumulator for that pressure difference. We present results typical for a cycle that consists of discharging from 0.6 MPa to 0.3 MPa at a load resistance of 6.8 Ω . In this range we can expect an average efficiency of the take-off system of 6% (Figs. 6 and 12) and of the pumping cylinder of around 75% (Fig. 9 with $V_{dead} = 80$ mL). Multiplying these efficiencies we get a total efficiency of 4.5%. From measurement results we see that for charging the accumulator from 0.3 MPa to 0.6 MPa we must exert an amount of 5015 J of mechanical energy (not shown in figure). When the accumulator is discharged back to 0.3 MPa the pneumatic motor consumes 1960 J of pneumatic power. That means the production of pneumatic power had an efficiency of only 39%. This is clearly less than expected from the theoretical model. The compression does not happen perfectly isothermal, as observed from Fig. 14. This can explain some of the difference between theoretical and actual pumping efficiency. Another effect reducing the efficiency could be back flow through the high pressure check valve. These issues should be addressed in future developments. The air motor and generator unit produce 100 J of electrical energy which is consumed by the electrical load. This gives a total measured cycle efficiency of only 2%. One cycle of charging and discharging takes 182 + 21 s at a sufficient wave height to fully actuate the piston and a wave period of 5 s. At these conditions the average electrical power output is approximately 0.49 W.

5. Discussion

We developed and modeled a functioning wave energy converter with pneumatic power-train and assessed the energy losses in each of its components. The modeling gives valuable practical insight into losses of various parts of pneumatic drive trains. Pumping efficiency, at least theoretically, is quite high ($\sim 70\%$ – 90%) due to the slow compression rate that allows heat exchange. The main factor reducing the compression efficiency is dead volume. In practice, the measurements indicate additional losses probably caused by back-flow through the high pressure check valve. Line losses can be neglected compared to the main source of losses, the vane motor. The vane motor has a maximum efficiency of 13.6%. The generator and belt transmission efficiency increases with torque and speed and electrical load. It can be up to 57%. The operating point for the unit consisting of pneumatic motor

coupled with the generator, however only allows for a combined efficiency of maximally $\sim 6.1\%$ depending on pressure supply and electrical resistance. Experimental results validate the model predictions well. The cycle-averaged efficiency of the power transmission from mechanical excitation into electrical consumer load is 2% for typical electrical loads. This means, only 0.5 W of the harvested 20 W of wave power could be harnessed into electrical power output. For the sake of comparison, photo voltaic cells can produce 600 Wh/day at the same surface area, assuming 5 kWh effective solar energy per day and 12% system efficiency.

The efficiency of the setup could be improved by reducing the dead volume in the pumping cylinder or finding an alternative air motor with higher efficiency. However, it is not the aim of this study to optimize a pneumatic power transmission for a wave energy converter. Rather we provide a case study for the assessment of pneumatic power transmissions for wave energy converter power take-offs that could be instructional for similar projects.

With only a pneumatic cylinder exposed to the saltwater environment, the power take-off is simple and rugged. It is lightweight, portable and deployable by only two people within 20 min provided that anchored threaded bolts are prepared on the site of installation. The setup is comparatively cheap as well. Table 2 lists the components and their cost without instrumentation.

The motor is by far the component with the lowest efficiency and the highest cost. Therefore, to increase the power yield, a more efficient motor is required. For a small scale application this is challenging. To our knowledge, no better commercially available alternative for such low power requirements exists. A micro air turbine could offer slightly better performance. Peirs et al report a peak efficiency of 18.4% for a 25 W custom designed microturbine [23]. The speed of a micro air turbine is very high ($\sim 100,000\text{ rpm}$) so that reduction gears would have to be used, which might reduce the total efficiency slightly.

6. Conclusion

In conclusion, we presented the modeling of a pneumatic wave energy converter power take-off. Given the low efficiency, we determined what is the basis for discussion of the results. However, it was not the aim of the project to demonstrate the high efficiency of pneumatic drive trains. Our prototype is suitable for exploring and teaching wave energy harvesting techniques. The prototype serves very well as a demonstrator for the principle of wave energy conversion and the challenges of harvesting energy from waves. While the goal of harvesting energy is clearly achieved, we gained practical insight into the challenges of converting a slow motion, high force energy source into useful energy. Some of them are:

- Optimization of wave interface to increase power output.
- Mechanical design must take into account large ratio between maximum average power and forces.
- Adaptability to wave conditions through choice of pumping pressure level.
- Control of power take-off with respect to average performance rather than to peak performance.

Besides practical insights into wave energy conversion, this can be used as a case study for the assessment of energy efficiency of a complete pneumatic power-train.

Acknowledgments

We gratefully acknowledge funding by the American University of Beirut and the Angela and Munib Masri Foundation. We also acknowledge the work of Khaled El Monajjed, Omar Hussein Safadi, Hadeel Hijazi, Ayman Ghalayini, Mostafa Itani, and Omar Malas on designing and manufacturing the mechanical, electrical and pneumatic setup as part of their undergraduate senior year projects.

Appendix A. Parameter values of setup

Table 3

Nomenclature.

Symbol	Comment	Unit
D_{piston}	Piston diameter	m
D_f	Friction damping constant	N.m.s
D_{tube}	Tube diameter	m
$F_{\text{cyl.c}}$	Coulomb friction of cylinder	N
K	Correction factor for pneumatic resistances	–
K_{emf}	Electromotive force constant	V.s/rad
L	Losses	W
l_{equiv}	Equivalent length	m
\dot{m}	Mass flow	kg/s
p	Pressure	Pa
p_{acc}	Accumulator pressure	Pa
p_{atm}	Atmospheric pressure	Pa
P_{air}	Air power	W
$P_{\text{arm.mech}}$	Armature mechanical power	W
$P_{\text{cyl.mech}}$	Mechanical input power to piston	W
R_m	Armature resistance	Ω
R_w	Wiring and connector resistance	Ω
$s_{\text{p.max}}$	Maximum stroke of piston	m
T_{atm}	Atmospheric temperature	K
T_{gen}	Generator shaft torque	Nm
$T_{\text{gen.c}}$	Coulomb friction	Nm
$T_{\text{gen.fric}}$	Total generator friction	Nm
T_p	Period of wave	s
V_{dead}	Dead volume in cylinder	
V_{emf}	Electromotive force	V
V_p	Velocity of piston	m/s
$V_{1,2,3,4}$	Cylinder volume in state 1–4	m^3
W	Work	V
ω	Shaft speed	rad/s

Table 4

Parameter values of setup.

Symbol	Comment	Unit
$s_{\text{p.max}} = 0.125$	Maximum piston stroke	m
$D_f = 0.0012$	Rotational damping of DC generator	N.m.s
$D_{\text{piston}} = 0.1$	Piston diameter	m
$D_{\text{pistonrod}} = 0.025$	Piston rod diameter	m
$K_{\text{emf}} = 0.296$	Electromotive force constant	Vs
$K_m = 0.296$	Motor torque constant	Nm/A
$n = 1.4$	Ratio of specific heat constants of air	–
$p_{\text{atm}} = 1 \cdot 10^5$	Atmospheric pressure	Pa
$R_m = 2.6$	Armature resistance	Ω
$R_w = 3.1$	Slip ring and wiring resistance	Ω
$s_{\text{p.max}} = 0.125$	Maximum piston stroke	m
$T_{\text{atm}} = 298.13$	Atmospheric temperature	K
$T_{\text{gen.c}} = 0.116$	Static friction torque	Nm
$T_{\text{period}} = 5$	Wave period	s
$V_{\text{acc}} = 5$	Volume of accumulator	L
$V_{\text{dead}} = 11 \cdot 10^{-6}$	Dead volume of cylinder	L
$V_1 = 0.913 \cdot 10^{-3}$	Max volume of cylinder	m^3

References

- [1] B. Drew, A.R. Plummer, M.N. Sahinkaya, A review of wave energy converter technology, *Proc. Inst. Mech. Eng. Part A: J. Power Energy* 223 (8) (2009) 887–902.
- [2] B. Czech, P. Bauer, Wave energy converter concepts: design challenges and classification, *Industrial Electronics Magazine*, 6 (2), IEEE, 2012. 4–16.
- [3] Y. Kamizuru, Development of hydrostatic drive trains for wave energy converters: a model-based assessment of performance efficiency and cost, Shaker, 2014.
- [4] S.O. strategic initiative for ocean energy, *Ocean energy: state of the art*, Tech. rep., 2014.
- [5] Medatlas Group, *Wind and wave atlas of the Mediterranean Sea*, W.E.A.O. Research Cell, 2004.
- [6] N. Kabbara, Wind and wave data analysis for the Lebanese coacoast area – preliminary results, *Lebanese Sci. J.* 6 (2) (2005) 45–56.
- [7] M. Folley, R. Curran, T. Whittaker, Comparison of (LIMPET) contra-rotating wells turbine with theoretical and model test predictions, *Ocean Eng.* 33 (89) (2006) 1056–1069.
- [8] R.P.F. Gomes, J.C.C. Henriques, L.M.C. Gato, A.F.O. Falco, Design of a floating oscillating water column for wave energy conversion, in: *The European Wave and Tidal Energy Conference 2011*, 2011.
- [9] B.M. Count, E.R. Jefferys, Wave power, the primary interface, in: *Proceedings of the 13th Symposium in Naval Hydrodynamics* The Shipbuilding Research Association of Japan, Tokyo, October 1980, Paper 8, 1980, pp. 1–10.
- [10] J. Falnes, *Ocean Waves and Oscillating Systems: Linear Interactions Including Wave-Energy Extraction*, Cambridge University Press, 2005.
- [11] J. Falnes, A review of wave-energy extraction, *Mar. Struct.* 20 (4) (2007) 185–201.
- [12] J.H. Todalshaug, Practical limits to the power that can be captured from ocean waves by oscillating bodies, *International Journal of Marine Energy* 34 (0) (2013) e70–e81. Special Issue Selected Papers – {EWTEC2013}.
- [13] DEPRAG, Air motors – customized drive solutions. URL <<http://www.depragusa.com/files/catalogs/D6000en.pdf>>.
- [14] M. Cai, K. Kawashima, T. Kagawa, Power assessment of flowing compressed air, *J. Fluids Eng.* 128 (2005) 402–405.
- [15] P. Beater, Modelling and control of pneumatic vane motors, *Int. J. Fluid Power* 5 (2004) 7–16.
- [16] P. Moreton, Chapter 1 – brushed DC motors, in: P. Moreton (Ed.), *Industrial Brushless Servomotors*, Newnes Power Engineering Series, Newnes, Oxford, 2000, pp. 1–27.
- [17] H. Falkmann, Compressed air distribution, in: S. Andersson, G. Bevegut, J. Eckersten, G. Ek, B. Kalladin (Eds.), *Atlas Copco Air Compendium*, Atlas Copco AB, Stockholm, 1975, pp. 473–494.
- [18] J. Eckersten, Simplified flow calculations for pneumatic components, in: S. Andersson, G. Bevegut, J. Eckersten, G. Ek, B. Kalladin (Eds.), *Atlas Copco Air Compendium*, Atlas Copco AB, Stockholm, 1975, pp. 183–192.
- [19] P. Beater, *Pneumatic Drives – System Design, Modelling and Control*, Springer, 2007.
- [20] A. Barber, Section 3 – energy and efficiency, in: A. Barber (Ed.), *Pneumatic Handbook*, eight ed., Butterworth–Heinemann, Oxford, 1997, pp. 129–161.
- [21] H. Fleischer, *Pneumatic Drives – System Design, Modelling and Control*, Mcgraw-Hill, 1995.
- [22] A. Al-Ibrahim, D. Otis, Transient air temperature and pressure measurements during the charging and discharging processes of an actuating pneumatic cylinder, in: *Proceedings of the 45th National Conference on Fluid Power*, Chicago, 1992, pp. N92–16.1.
- [23] J. Peirs, D. Reynaerts, F. Verplaetsen, Development of an axial microturbine for a portable gas turbine generator, *J. Micromech. Microeng.* 13 (2003) 190–195.